3704 *Chem. Mater.* **2010,** *22,* 3704–3711
DOI:10.1021/cm100653q

CHEMISTRY OF MATERIALS
Article

N-Doped Titanium Monoxide Nanoparticles with TiO Rock-Salt Structure, Low Energy Band Gap, and Visible Light Activity

Pardis Simon,[†] Bruno Pignon,[†] Baoji Miao,[†] Servane Coste-Leconte,[‡] Yann Leconte,[†] Sylvie Marguet,[†] Pascale Jegou,[§] Brigitte Bouchet-Fabre,[†] Cécile Reynaud,[†] and Nathalie Herlin-Boime*[,†]

[†]*CEA, IRAMIS, SPAM, LFP (CEA-CNRS URA 2453), 91191 Gif/Yvette, France,* [‡]*INSTN-UESMS, CEA Saclay, 91191 Gif/Yvette, France, and* [§]*CEA, IRAMIS, SPCSI, 91191 Gif/Yvette, France*

Received March 3, 2010. Revised Manuscript Received May 17, 2010

Titania nanoparticles are widely studied for photoconversion processes where combining high surface area, charge transport properties, and chemical stability is meaningful. To enhance the conversion efficiency, new compounds with reduced band gap are actively researched to utilize the visible part of the solar spectrum. Some narrowing of the gap can be observed when doping titania with nitrogen, leading to suboxide species. Using laser pyrolysis, we have synthesized for the first time true titanium monoxide TiO nanoparticles with a rock-salt crystallographic structure. The as-formed nanoparticles of black color contain carbon which can be removed by soft annealing under air while maintaining the presence of the TiO phase. These nanoparticles exhibit a very large shift of the light absorption threshold, up to 1.2 eV toward visible range, compared to the anatase form of titania. XPS analysis allows discussion of the role of nitrogen in the formation of this phase and its optical properties. First results indicate efficient photoactivity under UV and visible irradiation.

Introduction

Titania has been the subject of studies for a long time because of applications as pigments in painting, cosmetics, or catalysis and is still intensively studied in connection with the recent fields of renewable energy (solar cells,[1,2] photo electrochemical splitting of water into hydrogen and oxygen[3,4]) or photocatalysis for degradation of organic pollutants.[5,6] However, because of its wide band gap (3.2 eV for the anatase form), absorption of solar light occurs mainly in the ultraviolet domain which limits the development of TiO_2 based devices. Therefore, synthesis of modified TiO_2 products with improved absorption in the visible region remains a major challenge. Doping titania with various heteroelements (C, N, S, F, P, Fe, ...) appears to be an efficient way to fulfill this objective.[7−10] In particular, synthesis of N doped TiO_2 nanoparticles is an especially active field since the study of Asahi demonstrating, close to 2 eV, the appearance of a second optical threshold attributed to a $TiO_{2-x}N_x$ structure and correlated to an enhanced photocatalytic activity.[7,11−13] Synthesis of N-doped thin films or powders, mainly with anatase as major crystalline form, are obtained by various methods such as annealing under NH_3 flow at high temperature,[7,11,14] decomposition of nitrogen metal−organic precursors,[15] sol−gel methods,[16] ion implantation,[17,18] and thin films deposition.[19] An alternative way for the narrowing of the optical band gap is the production of suboxide species, as shown in several papers devoted to TiO_{2-x} thin films.[20] The synthesis of suboxide powders is also reported in the literature, for example, by chemical methods,[21]

*To whom correspondence should be addressed. E-mail: nathalie.herlin@cea.fr.

(1) O'Regan, B.; Gratzel, M. *Nature* **1991**, *353*, 737.
(2) Grätzel, M. *Nature* **2001**, *414*, 338.
(3) Fujishama, A.; Honda, K. *Nature* **1972**, *298*, 37.
(4) Khan, S. U. M.; Akikusa, J. *Int. J. Hydrogen Energy* **2002**, *27*, 863.
(5) Hermann, J. M.; Duchamp, C.; Karkmaz, M.; Hoai, B. T.; Lachbav, H.; Puzenat, E.; Guillard, C. *J. Hazard. Mater.* **2007**, *146*, 624.
(6) Varghese, O.; Paulose, M.; LaTempa, T.; Varghese, G. C. *Nano Lett.* **2009**, *9*(2), 731.
(7) Asahi, R.; Morikawana, T.; Ohwaki, T.; Aoki, K.; Taga, Y. *Science* **2001**, *293*, 269.
(8) Teoh, W.; Amal, R.; Mädler, L.; Pratsinis, S. *Catal. Today* **2007**, *120*, 203.
(9) Yu, J.; Yu, J.; Ho, W.; Jiang, Z.; Zhang, L. *Chem. Mater.* **2002**, *14*, 3808.
(10) Zhou, M.; Yu, J. *J. Hazard. Mater.* **2008**, *152*, 1229.
(11) Burda, C.; Lou, Y. B.; Chen, X. B.; Samia, A. C. S.; Stout, J.; Gole, J. L. *Nano. Lett.* **2003**, *3*, 1049.
(12) Sathish, M.; Viswanathan, B.; Viswanath, R.; Chinnakonda, S.; Gopinath, S. *Chem. Mater.* **2005**, *17*, 6349.
(13) Mrowetz, M.; Balcerski, W.; Colussi, A. J.; Hoffmann, M. R. *J. Phys. Chem. B* **2004**, *108*, 17269.
(14) Peng, F.; Cai, L.; Huang, L.; Yu, H.; Wang, H. *J. Phys. Chem. Solids* **2008**, *69*, 1657.
(15) Belver, C.; Bellod, R.; Fuerte, A.; Fernandez Garcia, M. *Appl. Catal., B* **2006**, *65*, 2499.
(16) Venkatachalan, N.; Vinu, A.; Anandan, S.; Arabindo, B.; Murugesan, V. *J. Nanosci. Nanotechnol.* **2006**, *6*, 2499.
(17) Diwald, O.; Thompson, T. L.; Goralski, E. G.; Walck, E. D.; Yates, J. T. *J. Phys. Chem. B* **2004**, *108*, 52.
(18) Ghicov, A.; Macak, J. M.; Tsuchika, H.; Kunze, J.; Haueblein, V.; Kleber, S.; Schumuki, P. *Chem. Phys. Lett.* **2006**, *419*, 426.
(19) Guillot, J. Titanium oxinitride thin films: the reactivity as an original physico-chemical characterization method. Ph.D. Thesis , University of Burgundy, Dijon, France, 2002; http://tel.archives-ouvertes.fr/tel-00101455/en/
(20) Wang, Y.; Qin, Y.; Li, G.; Cui, Z.; Zhang, Z. *J. Cryst. Growth* **2005**, *282*, 402.
(21) Shibuta, D.; Koboyashi, S.; Yoshizumi.; Arai, H. U.S. Patent 4,668,501, 1987.

Published on Web 05/27/2010

electrochemical reduction,[22] flame synthesis,[23] laser pyrolysis,[24] and mechanochemical synthesis.[25] In this latter study, TiO_x ($0.92 < x < 1.19$) in cubic or monoclinic form was identified by X-ray diffraction (XRD) after mechanochemical treatment of Ti and TiO_2 (rutile) powder mixtures. A true cubic TiO structure was obtained after milling of an equimolar mixture of Ti and TiO_2 powders but no optical properties were reported. Commercial powders referred as TiO (Alfa Aesar: 042939 Titanium(II)-oxide, 99.9% (metal basis) CAS 12137−20−1; Sigma Aldrich 042939 Titanium(II)oxide, 99.9% (metal basis) CAS 12137−20) are available and indeed exhibit the TiO average stoichiometry. However, these products contain many TiO_x polymorphs, and the optical properties are not interesting in terms of visible absorption.

We have recently demonstrated the efficient synthesis of TiO_2 and N-doped TiO_2 nanoparticles by the laser pyrolysis method[26] which offers the advantage of a continuous process where the particles are produced in a streamflow with a flame. This method is very versatile, and the proportion of anatase and rutile phases in the final products can be controlled over a large range (5 to 90%). The N-doped TiO_2 nanoparticles with N weight content of 3% were obtained by the addition of NH_3 in the reaction zone. The UV transmission spectrum exhibits two energy thresholds as observed in the Asahi study.[7] This result was obtained at moderate temperature of reaction (driven by the laser power density in the interaction zone), and it is worthwhile to underline that anatase was the only crystalline phase identified in this powder.

Taking advantage of the laser pyrolysis versatility, we explore in the present work a new range of experimental conditions. In particular, we focus on the effect of increasing the reaction temperature by increasing the laser power density and the time of residence in the reaction zone. The objective is to favor the synthesis of suboxide species through the presence of a reducing atmosphere in the NH_3-rich reaction zone and increase the nitrogen content in the powder. In these conditions, we show in the following that the resulting product is a new form of Ti(O, N) nanoparticles where the major crystalline phase is titanium monoxide TiO with a rock-salt structure, as identified by XRD, together with a minor anatase phase. These results are analyzed with the help of X-ray Photoelectron Spectroscopy (XPS). To our knowledge, this work reports the first direct synthesis of nanocrystalline TiO, and it is obtained in gram quantities in one synthesis experiment. Moreover, the optical absorption spectrum of this original product and its evolution as a function of annealing treatments are also reported. It shows a remarkable shift of the light absorption threshold as large as 1.2 eV toward visible range as compared to the anatase form. Finally, very promising photoactivity is demonstrated under visible light.

Experimental Section

Nanoparticles were synthesized in a cw-CO_2 laser beam using liquid titanium(IV) isopropoxide (TTIP) (Sigma Aldrich, 97%) as a precursor. The experimental setup was very similar to the one described previously,[26] but the experimental parameters have been modified to achieve higher temperature in the reaction zone. A TTIP aerosol was obtained by using an ultrasonic spraying technique (Pyrosol process). The produced droplets were carried out to the reaction chamber by a 750 sccm N_2 carrier gas flow through a 6 mm diameter nozzle. N_2 was chosen here as carrier gas in place of Helium used in to our previous study[26] because N_2 has a much lower thermal diffusivity and allows better confinement of reactive species. A low flow of gaseous ammonia (100 sccm) was introduced just before the exit of the inlet nozzle. Because the NH_3 laser absorption is high, no addition of sensitizer gas was needed. The flow of the reactants mixture was orthogonal to the focused laser beam, and the total gas flow was decreased by a factor of 2.8 which allows longer time of residence of reactive species in the reaction zone and better decomposition of the reactants. This is expected to favor the production of reducing species issued from the decomposition of NH_3 and the incorporation of N atoms in the powders. The pressure reaction was fixed to 740 Torr in the presence of the carrier gas flow, and the laser power was 1000 W. In the present study, 6.35 g/h of liquid TTIP were consumed to produce 1.44 g/h of AF powders, the maximum chemical conversion from TTIP to TiO_2 is calculated as 28%, meaning an effective yield of 81%.

Nitrogen mass concentration was determined by the Dumas method by the SGS company. The morphology was examined by transmission electron microscopy (TEM). To obtain images of the nanoparticles, nanopowders were dispersed in ethanol by using an ultrasonic probe. A drop of the solution was placed onto a carbon-film-coated TEM grid and allowed to dry. After that, nanoparticles were imaged using a Philips TEM CM12. Size distribution was estimated by counting 150 particles. Powder XRD patterns were recorded on a Siemens D5000 using a Bragg−Brentano diffractometer in $\theta-2\theta$ geometry and Cu−Kα radiation with a secondary monochromator. The 2θ angle ranged from 20° to 80° with a step size of 0.02° (2θ) and a counting time of 10s/step. Average crystallite sizes for the (hkl) plane were evaluated thanks to Scherrer's formula: $D_{(hkl)} = \kappa\lambda/\beta\cos(\theta)$,where κ is the shape factor, λ the X-ray wavelength of Cu(Kα) radiation, β the full width at half-maximum (fwhm) of the ($h\,k\,l$) peak corrected for instrumental broadening, and θ is the diffraction angle. All the patterns were adjusted thanks to a NaCl internal standard (Sigma Aldrich S7653), and the crystallite sizes were calculated using the TiO (200) peak.[27] XPS was run on a Kratos Analytical Axis Ultra DLD spectrometer with monochromatic Al Kα X-ray ($h\nu = 1486.6$ eV). The energy resolution of the spectrometer was set at 0.35 eV at a pass energy of 20 eV. Binding Energy was calibrated with respect to Au 4f7/2 core level at 84 eV. In the decomposition of the Ti 2p levels, the ratio between 1/2 and 3/2 surfaces was fixed at 2/3−1/3 and the width ratio was fixed at 1−1, and the intensities were each component of 1/2 peak is shifted from 3/2 peak of 6.0 eV. The curves used in the fit were a mixture of Gaussian and Lorentzian

(22) Wainer, E.; Heights, C.; Sibert, M. E.; Heights, G. U.S. Patent 2,707,168, 1950.
(23) Teleki, A.; Pratsinis, S. E. *Phys. Chem. Chem. Phys.* **2009**, *11*, 3742.
(24) Maskrot, H.; Herlin-Boime, N.; Leconte, Y.; Jursikova, K.; Reynaud, C.; Vicens, J. *J. Nano. Res.* **2006**, *8*, 351.
(25) Velkovic, I.; Poleti, D.; Zdujic, M.; Karanovic, L.; Jovalekoc, C. *Mater. Lett.* **2008**, *62*, 2769.
(26) Pignon, B.; Maskrot, H.; Guyot-Ferreol, V.; Leconte, Y.; Coste, S.; Gervais, M.; Pouget, T.; Reynaud, C.; Tranchant, J. F.; Herlin-Boime, N. *Eur. J. Inorg. Chem.* **2008**, *6*, 883.
(27) Cullity, B. D. In *Elements of X-ray Diffraction*. Addison-Wesley: Reading, MA, 1978.

curves with a 20% Lorentzian contribution. Band gap measurements were made using the transformed diffuse reflectance technique according to the Kubelka−Munk theory.[28] Diffuse reflectance spectra of the powders were measured on a UV−vis−NIR spectrophotometer (Jasco V-570), which was equipped with an integrating sphere assembly. A given amount of nanopowder was uniformly pressed in a powder holder (Jasco) and placed in the sample holder on an integrated sphere for the reflectance measurements. The reflectance data was converted to the absorption coefficient $F(R_\infty)$ values according to the Kubelka−Munk equation, that is, $F(R_\infty) = [(1 - R_\infty)^2/2R_\infty]$, where $F(R_\infty)$ is equivalent to the absorption coefficient. The absorption coefficient of an indirect semiconductor near the absorption threshold can be expressed as $\alpha = [B_i(h\nu - Eg)^2]/h\nu$, where Eg is the band gap of indirect allowed transition (eV), h the Planck's constant (J s), B_i the absorption constant, and ν is the frequency of the light (s^{-1}). Therefore, a transformed Kubelka−Munk function can be constructed by plotting $[F(R_\infty)]^{1/2}$ as a function of the energy of excitation source. This allows obtaining the band gap of the semiconductor[29,30] as the intersection of the tangent to the linear part of the curve with the energy axis. As the presence of carbon is a point discussed in this study, spectra were also recorded on mixtures of laser synthesized sized TiO_2 nanoparticles and measured amounts of nanosized amorphous carbon. The measurements are no more reliable and the measurement of a gap position is not possible as soon as the carbon content is higher than 0.5 wt %. Specific surface area was measured with a Micromeritics FlowsorbII 2300 using the BET (Brunauer−Emmett−Teller) method after degassing the samples for 1 h at 200 °C. The light induced activity was evaluated by measuring the evolution of methylene blue signal as a function of the excitation wavelength. Suspensions of nanopowder (P25 from Degussa and laser synthesized samples) in deionized water (Millipore) were prepared and sonicated with an ultrasonic tip during 30 min. Methylene blue solution was added (concentration 1 μmol/L) to the suspensions. After mixing in the dark, suspensions were irradiated with a constant photon flux at various wavelengths with a monochromatized Xenon arc fluorimeter (Fluorolog3, Horiba Jobin Yvon). The suspensions were kept under magnetic stirring during irradiation. The concentration of methylene blue as a function of irradiation time was deduced from the variation of the optical density of the suspension measured at 664 nm. At a given excitation wavelength, the concentration of nanopowder (TiO_2 P25 and laser synthesized samples) was adjusted to obtain the measurements at the same optical density (i.e., constant number of absorbed photons).

Results and Discussion

Figure 1a shows that the as-formed powder exhibits a black color as observed previously.[26] It is interpreted in terms of carbon incorporation in the powder because of the high level of decomposition of TTIP at high flame temperature. The carbon can be easily eliminated by simple annealing treatment under air at 400 °C. In our previous work,[26] this heat-treatment induces only slight modification of the crystalline structure. The situation is very different here, since XRD analysis (Figure 2) shows a

Figure 1. Color evolution from AF sample (a) and as a function of annealing treatments under air at 300 (A300C) (b), 350 (A350C) (c), and 400 °C (A400C) (d).

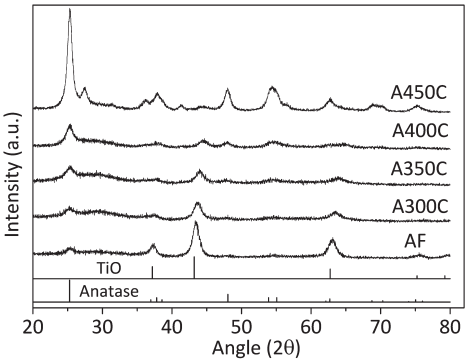

Figure 2. XRD diagrams before and after various annealing under air. References are JCPDS: TiO 077-2170; Anatase 021-1272; Rutile 21-1276. AF powder (crystallite diameter of TiO estimated from Scherrer is 9 nm); A300C, oxidation 6 h, 300 °C; A350C, 3 h, 350 °C; A400C, 3 h, 400 °C (crystalllite diameter of anatase estimated from Scherrer is 8 nm); A450C, 3 h 450 °C. The evolution of spectra after annealing from 300 to 400 °C shows an increase of the amorphous part of the sample. Note that no trace of TiC crystallization is observed.

significant evolution of the crystalline structure under heat-treatment at 400 °C. Indeed, the presence of a TiO phase, as discussed below, in the as-formed sample leads us to perform intermediate annealing treatments (below 400 °C) to maintain this phase, while decreasing the carbon content. During annealing treatments, the powder color evolves from black to light yellow going through brown and orange-brown intermediate colors as shown in Figure 1. The yellow color can be compared to the yellowish coloration observed in Asahi[7] and indicates the presence of N-doped TiO_2.

The N-content in the powders, determined by bulk chemical analysis, is very high in the as-formed sample (11.3 wt %) compared to the previous experiment (3 wt %[23]) and decreases down to 2.8 wt % after annealing at 400 °C under air (8.5% weight difference). The carbon content

(28) Lin, H.; Huang, C.; Li, W.; Ni, C.; Ismat Shah, S.; Tseng, Y. *Appl. Catal., B* **2006**, *68*, 1.
(29) Lee, S.; Jeon, C. *Chem. Mater.* **2004**, *16*, 4292.
(30) Simmons, E. *Appl. Opt.* **1975**, *14*, 1380.

Table 1. O/Ti and N/Ti Evolution As a Function of Temperature (Deduced from XPS Data) and Unit Cell Parameters (Å) Deduced from XRD for AF and Annealed at 300 (A300C), 350 (A350C), 400 (A400C), and 450°C (A450C) Samples

sample	O/Ti	N/Ti	TiO unit cell parameter, a/Å	crystallite diameter obtained from the main peak (nm)
AF	1.3	0.5	4.176	TiO, 9.0
A300C	1.9	0.3	4.139	TiO, 8.0
A350C	1.9	0.2	4.113	TiO, 8.0
A400C	1.9	0.1	4.069	TiO, 8.3 anatase,7.3
A450C	1.9	0.07		anatase, 10.9 rutile, 10.1

can be deduced from the weight gain under annealing, found equal to 4.5%. Supposing TiO as the only titanium-containing phase in the as-formed sample, full oxidation to TiO_2, expected after annealing at 400 °C under air, should increase the weight by 25%. The missing 20.5% can be attributed reasonably to departure of nitrogen (8.5%) and to carbon oxidation, corresponding then to about 12% carbon content in the as formed (AF) powder which is comparable to other measurements obtained on samples synthesized in close conditions and found to be around 10%.

XPS analysis allows us to deduce O/Ti and N/Ti ratios (Table 1). A significant increase in O content and a progressive decrease in N content were observed with annealing temperature. The O/Ti ratio in the as-formed powder is higher than 1, which indicates that the sample contains more oxygen compared to the crystalline TiO phase seen by XRD, indicating the presence of more oxidized species in an amorphous phase. Surprisingly, the O/Ti ratio is equal to 1.9 at a temperature as low as 300 °C meaning that the chemical composition is already close to the dioxide stoichiometry, a point which will be discussed below.

X-ray Diffraction (XRD) patterns presented in Figure 2 appear very different from the classical anatase and rutile crystallographic phases of TiO_2. By comparison with the peak positions given by ICDD-PDF databases, it appears that the main crystallographic phase is TiO in a rock-salt NaCl structure together with a minor TiO_2 anatase contribution, in strong contrast with our previous work[23] where only anatase was observed. Moreover, the unit cell parameter obtained for the AF sample is 4.18 Å, in agreement with the value reported in the literature for this phase.[22] The highly reduced TiO phase observed here shows that at high temperature, the dissociation of NH_3 in the reaction zone leads to a reducing atmosphere very efficient to produce highly suboxide species in a one step process. All other experiments performed in the laboratory, without NH_3, with varying reactant flow and even at the highest laser power have never shown such atypical TiO phase. This indicates that the presence of NH_3 (or possibly another source of reducing species) in the reactive phase, together with a high reaction temperature, is as an essential parameter to produce and stabilize the TiO phase. XRD diagrams were recorded at intervals of 6 months on powders kept in ambient conditions; no modification could be detected in AF nor annealed samples.

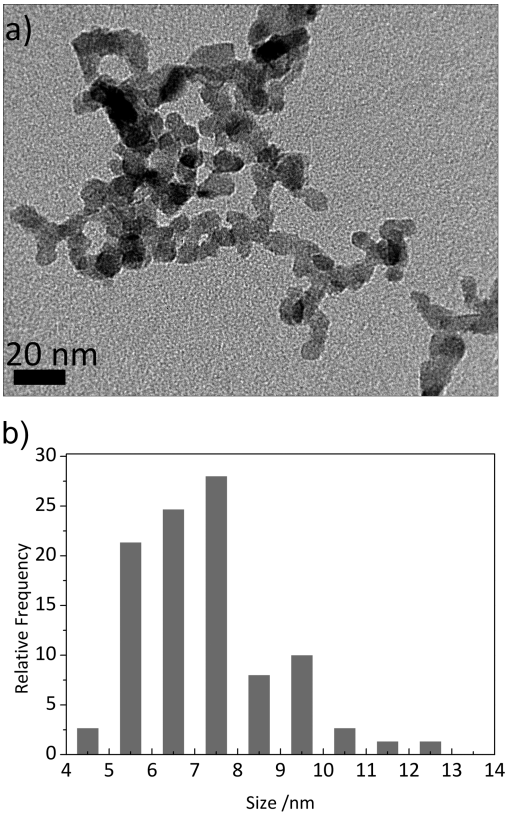

Figure 3. (a) Typical morphology and (b) size distribution (count on 150 nanoparticles) of AF sample.

In all the XRD patterns (Figure 2), the main anatase peak appears at the exact position expected for anatase while the (200) peak attributed to TiO in the AF powder is progressively shifted toward higher θ values (from 2θ = 43.3° to 2θ = 44.5°) with increasing temperature, corresponding to a decrease of the unit cell parameter from 4.18 to 4.07 Å (Table 1). This is interpreted in terms of increasing x value in TiO_x samples ($0.5 < x < 1.4$)[31] while keeping the same NaCl rock salt like structure. The difference between XRD, which still indicates the presence of the suboxide structure, and XPS, which gives a total O/Ti ratio close to 2 after treatment at a temperature as low as 300 °C, could be related to surface to volume effects. Oxidation may occur first at the surface and could explain the high O/Ti ratio measured from XPS. However, Figure 3 shows TEM plate of AF powder. The general morphology is in a chain like manner, and the average size of the nanoparticles is as small as 7 nm, in good agreement with the average crystallite size of 9 nm (Table 1) determined by Scherrer's formula on the (200) reflection of TiO phase. In this size range, XPS is also expected to be sensitive to the core chemical composition. Another explanation could come from the presence of amorphous material in large amounts, since XPS is sensitive to both amorphous and crystalline material while XRD is more sensitive to crystalline phases. Indeed, in Figure 2 an amorphous signal underlying the TiO and TiO_2 XRD peaks is apparent after annealing at

(31) Andersson, S.; Collén, B.; Kuylenstierna, U.; Magnéli, A. *Acta Chem. Scand.* **1957**, *11*, 1641.

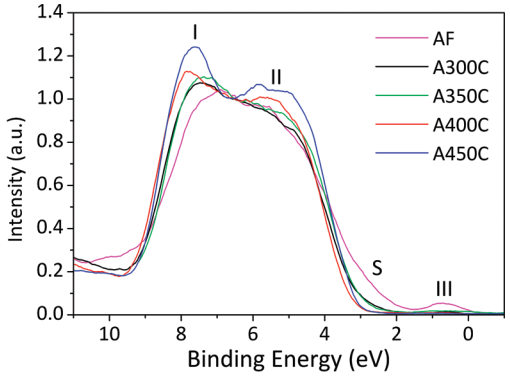

Figure 4. Evolution of the valence band extracted from XPS measurements as a function of annealing treatments. The spectra are decomposed in different components labeled I, II, III and a shoulder labeled S. The zero corresponds to the Fermi level (the spectra are normalized to the low energy point between components I and II).

temperatures from 300 to 400 °C, which could be attributed to an intermediate state where a part of TiO has been oxidized and is not yet crystallized in a TiO_2 phase. The XRD diagrams also indicate that we probably do not have a crystalline TiO_xN_y structure (or it is below the detection limit). In this latter case, some peaks should be observed between TiN and TiO. Therefore, we conclude that nitrogen is inserted in the TiO lattice corresponding to a Ti(O, N) material. In agreement with the chemical evolution, XRD shows an increase in the ratio of the anatase TiO_2 to suboxide TiO peaks intensity with increasing temperature up to 400 °C. After annealing at 450 °C, the anatase crystallization is pronounced (higher signal/noise ratio, sharper peaks) and the rutile phase begins to appear. Let us note that Kim[32] observed the amorphous-anatase transition at 500 °C and anatase-rutile at 650 °C for nanocrystallites in the range 10−20 nm. The very small size (< 10 nm) of our nanoparticles as well as the insertion of heteroatoms can lead to significantly lower transition temperatures (as described for V doped TiO_2[33]).

The structural evolution of these Ti(O, N) samples has been explored by XPS (Figures 4, 5, and 6) for the AF and annealed nanoparticles (same set of samples as shown previously). In Figure 4, the valence band of the samples is mainly characterized by a massif extending from 3 to 9 eV under the Fermi level which evolves significantly under annealing treatments. The decomposition into different peaks is given in Table 2. According to Bartkowski et al,[34] this large band is composed mainly of O(2p) states. The high binding energy side (component I) of this valence band feature is centered at 6.7 eV for the AF powder is attributed to σ bonding orbitals, with a contribution of Ti(3d and 4p) states, the low energy side (component II) centered at 4.4 eV being π non-bonding orbitals. With increasing temperature, this band tends to shift toward higher energies and to be more structured,

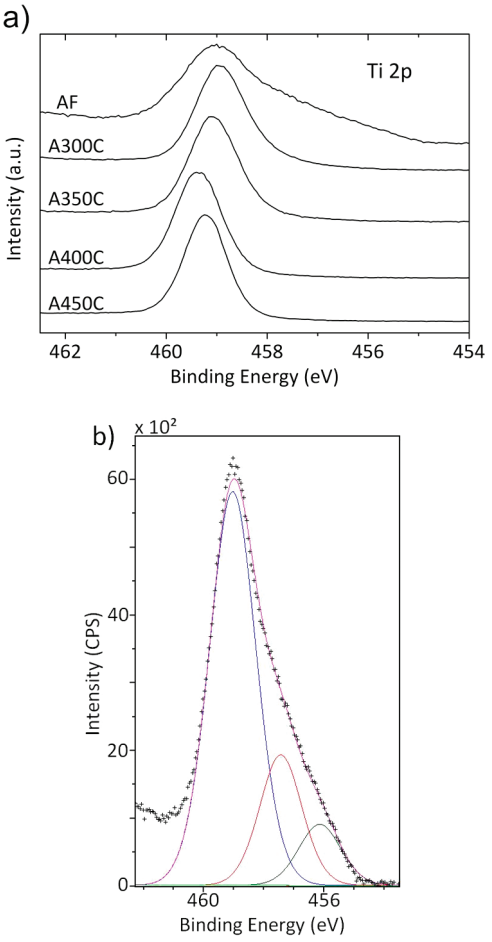

Figure 5. (a) XPS Ti 2p line of AF and annealed Ti(O, N) samples. For easier presentation, the curves haves been shifted; (b) Ti 2p line of AF Ti(O, N) sample. The reconstruction of the 3/2 component gives three peaks centered at 459.1 eV, 457.1, and 456.3 eV corresponding to different oxidation states of titanium, respectively Ti^{4+}, Ti^{3+}, and Ti^{2+}.

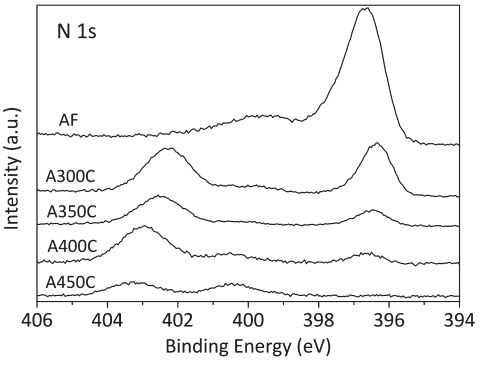

Figure 6. XPS N-1s line for AF and annealed Ti(O,N) samples. One evolves from a structure dominated by a peak at 396.7 eV in the AF powder to a structure dominated by a component at 402.8 eV in the sample annealed at 400 °C with a progressive appearance of a new band at 400.0 eV. The signal-to-noise ratio decreases in correlation with the total decrease of N content after annealing at higher temperature.

finally resembling the anatase valence band.[35] Therefore, the relative contribution of the non-bonding orbitals is the higher in the as-formed powder, and the bonding orbitals contribution increased with heat-treatment.

(32) Kim, E.; Hahn, S. *Mater. Lett.* **2001**, *49*, 244.
(33) Depero, L.; Bonzi, P.; Musci, M.; Casale, C. *J. Sol. State Chem.* **1994**, *111*, 247.
(34) Bartkowski, S.; Neumann, M.; Kurmaev, E.; Fedorenko, V.; Shamin, S.; Cherkashenko, V.; Nemnonov, S.; Winiarski, A.; Rubie, D. *Phys. Rev. B* **1997**, *56*, 10656.
(35) Tang, H. Ph.D. Dissertation, Ecole Polytechnique Fédérale de Lausanne (EPFL), Lausanne, Switzerland, 1994; p 55.

Table 2. Result of Valence Band Decomposition[a]

	peak I	peak II	peak III
AF	6.74	4.43	0.66
A300C	7.36	5.12	
A350C	7.45	5.19	
A400C	7.72	5.38	
A450C	7.70	5.31	

[a]Binding energy is given in eV.

Table 3. Result of Ti 2p Levels Decomposition in Gaussian-Lorentzian Components[a]

	Ti $2p_{3/2}$			Ti $2p_{1/2}$		
	Ti^{2+}	Ti^{3+}	Ti^{4+}	Ti^{2+}	Ti^{3+}	Ti^{4+}
AF	456,3	457,7	459,1	462,3	463,7	465,1
A300C	456,8	458,1	459,2	462,8	464,1	465,2
A350C			459,3			465,0
A400C			459,3			465,1
A450C			459,2			464,9

[a]Binding energy is given in eV.

Table 4. Peak Deconvolution of N1s Core Levels (Figure 6)[a]

	N1	N2	N3	N4	N5
	Ti (N, O)	N−Ti	N−Ti or N−C	N−O−	(N−O_2−)
AF	396.6	397.4	399.6		
A300C	396.6			400.4	402.5
A350C	396.8			400.5	402.9
A400C	396.7			400.5	403.0
A450C	396.3		398.5	400.5	403.2

[a]Binding energy is given in eV.

The valence band of the as-formed powder exhibits additional states (component III) centered at 0.66 eV, together with a shoulder, labeled S in Figure 4, on the low energy side of the massif, attributed to Ti(3d) states in TiO phase.[34] The shoulder component is still easily detected after annealing up to 350 °C. Its progressive elimination with increasing annealing temperature together with the splitting of the band can be interpreted in terms of progressive oxidation of TiO to TiO_2 in good agreement with XRD diagrams.

Regarding now the core levels, the N 1s, C 1s, O 1s, and Ti 2p have been recorded. In the following, we will discuss the detailed XPS spectra at the Ti and N levels (Figure 5 and 6 respectively, Tables 3 and 4) and comment briefly the O 1s and C 1s spectra (not shown). Concerning the C1s level, let us just note that it gives no indication of a possible Ti−C bonding expected at 281.7 eV.

Figure 5 (and Table 3) shows a strong evolution of the XPS Ti 2p line before and after annealing. The spectrum obtained for the AF sample exhibits a rather different shape from other spectra. The Ti $2p_{3/2}$ peak can be decomposed in three components centered at 459.1, 457.7, and 456.3 eV (Figure 5b and Table 3), interpreted in terms of different oxidation states of titanium from Ti^{4+} to Ti^{2+}.[14,36,37] It is worthwhile to note the absence of the TiN peak expected at 455.3 eV,[38] in agreement with the XRD data. The Ti^{2+} component at 456.3 eV corresponds to titanium monoxide TiO as observed by XRD. The Ti^{3+} component at higher energy (457.7 eV), corresponds to intermediate oxidation states such as suboxide surface state[39] and O−Ti−N bonding,[12,36] that can be found when the Ti cation is reduced because of the addition of nitrogen in the lattice of a Ti(O,N) structure and to the lower electronegativity of N compared to O.[12,36] The last component Ti^{4+} at 459.1 eV is due to the presence of the small anatase contribution (observed in XRD) and also to dioxide, probably at the grain surface[39] in an amorphous state as discussed above.

Under annealing, the Ti^{2+} and Ti^{3+} states disappear progressively, inducing a global shift of the peak, indicating an oxidation. The XPS spectrum after annealing at temperatures higher than 350 °C can be mainly interpreted in terms of O−Ti−O bonding (Ti^{4+}) with two main components at 465.0 ($2p_{1/2}$ component) and 459.3 eV ($2p_{3/2}$ component) (Table 3), corresponding to pure anatase and in agreement with XRD.[12]

The XPS data at the N 1s level (Figure 6 and Table 4) also show a strong evolution of the local environment with annealing treatments. Once again, the N 1s spectrum of the AF material is very different from all annealed samples. It is dominated by a peak at low binding energy (396.7 eV) attributed to N−Ti bonding in Ti(O, N).[19] This component regularly decreases with annealing temperature up to 450 °C where it almost disappears. The relative decrease of this peak seems related to the decreased content of bound N atoms.[7,38] In the AF sample, an additional type of bonding contributes to the core level centered at 399.6 eV which may be due to N−C bonding. After annealing, a third component appears at 402.3, slightly shifted toward higher energy with increasing temperature, and a minor component is located at 400.5 eV that may be attributed to N−O bonding (Table 4). The relative proportion of the minor component close to 400.5 eV increases with annealing. Both contributions are usually attributed to chemisorbed N_2.[11,12,14,37] However, the detailed attribution of these different peaks is still debated in the literature. Even if most authors[11,12,14,37] agree on the influence of oxidation on N atoms, Peng[14] attributes the minor component to a nitrogen substituting titanium (Ti−O−N−O or Ti−O−N−N) while Cong[37] relates it simply to a N substituting O in the TiO_2 phase. Important information of these XPS spectra is the relative decrease of the N−Ti bonding in Ti(O, N) peak (close to 396 eV) with increasing annealing temperature, in good agreement with the decrease of the Ti^{3+} signal (also attributed to Ti(O,N)) for temperatures higher than 350 °C in the Ti 2p spectra.

For all samples, (AF and annealed) the O 1s XPS spectra shows a major contribution centered at 530.7 eV corresponding to O−Ti bonding in the dioxide form.[40,41] An additional peak in the signal at higher binding energy

(36) Chen, X.; Burda, C. *J. Phys. Chem. B* **2004**, *108*, 15446.
(37) Cong, Y.; Zhang, J.; Chen, F.; Anpo, M. *J. Phys. Chem. C* **2007**, *111*, 6976.
(38) Saha, N. C.; Tomkins, H. C. *J. Appl. Phys.* **1992**, *72*, 3072.
(39) Göpel, W.; Rocker, G.; Feierabend, R. *Phys. Rev. B* **1983**, *28*, 3427.
(40) Peng, F.; Cai, L.; Huang, L.; Yu, H.; Wang, H. *J. Phys. Chem. Solids* **2008**, *69*, 1657.
(41) Chen, X.; Burda., C. *J. Phys. Chem. B* **2004**, *108*, 15446.

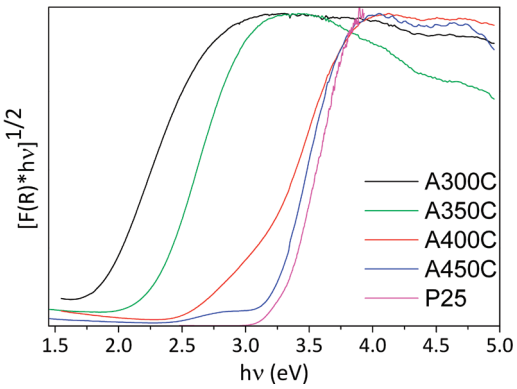

Figure 7. Transformed Kubelka−Munk (from diffuse reflectance spectra) function vs energy of the excitation source for different annealing temperatures compared with Degussa P25 reference. Determination of the optical bandgap is performed by reference to the indirect gap in semiconductors[44].

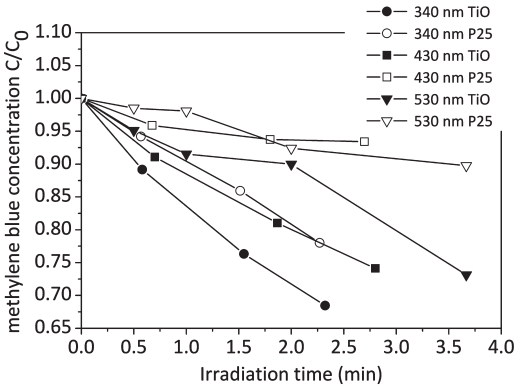

Figure 8. Light induced activity of A300C sample (filled symbols) and TiO2 sample (empty symbols) (P25 from Degussa) under UV-light irradiation (340 nm) (round shape symbols) and visible light irradiation (430 nm) (square symbols) or 530 nm (triangle symbols). In this Figure, the lines are only guides for the eyes. The concentration of methylene blue, measured at 664 nm, remains constant when exposed to light without nanopowders.

centered at 532 eV.is also present.[38,41−43] This component was first observed by Saha and Tomkins[38] and was most recently characterized by Gyorgy et al.[42] in their depth profiling study on TiN surfaces. Gyorgy et al. assigned it to the formation of oxidized Ti−N, which leads to the Ti−O−N structure and which remains consistent with our interpretation.

Figure 7 presents the significant evolution of UV−visible optical absorption spectra (deduced from diffuse reflectance spectra of the powders) as a function of annealing treatments. It shows a strong absorption in the visible range for the A300C and A350C samples. By contrast, the samples annealed at 400 and 450 °C exhibit a double threshold previously observed in N-doped TiO_2 samples[7] and attributed to the mixing of N and O 2p states.[7] Although TiO_2 was identified as the main crystalline structure for the sample annealed at 400 °C, its optical gap has not reached the value of anatase TiO_2: this is certainly due to the disorder remaining in the sample and to the high rate of surface atoms in these very small crystallites. By comparison of the spectra presented in Figure 7 with spectra obtained on samples containing known amount of nanosized amorphous carbon, we can say that the C content in the A300C sample is lower than 0.5 wt % and is still lower in the samples annealed at higher temperatures.

As compared with the samples annealed at 400 and 450 °C, the samples treated at 300 and 350 °C exhibit an unique optical gap (1.8 and 2.25 eV) largely shifted as compared to TiO_2 (Figure 7). By comparing the evolution of the optical gap with the evolution of the XPS spectra, especially the N−Ti contribution at 396 eV attributed to Ti(O, N) in the N 1s spectrum (Figure 6), it can be seen that the gap at lowest energy is observed for the more intense contribution at 396 eV. The gap appears shifted toward higher energy in correlation with the decrease of this contribution Ti(O,N) and the progressive decrease of the rock-salt crystalline phase. Therefore, we attribute the gap at 1.8 eV to a Ti(O,N) contribution in a rock-salt crystalline TiO phase. The gap is shifted with progressive oxidation to TiO_2.

For first evaluation of activity under light irradiation, a common test of evolution of methylene blue (MB) signal (detected at 664 nm) was performed with the A300C sample (S_{BET} = 128 m^2/g) and compared to the results of the same tests performed with a TiO_2 P25 (S_{BET} = 60 m^2/g) nanopowder, often used for its good photocatalytic performances. As noted in the Experimental Section, for a given excitation wavelength 340, 430, or 530 nm), the concentration of nanopowder was adjusted to to keep the same optical density for both TiO_2 P25 and laser synthesized samples. This means that the same number of photons was absorbed in the two experiments, which allows comparing them. Blank experiments were obtained by irradiating solutions of MB (without nanopowders) in the same condition (photon flux and exposure time). In the experiment time, no change could be observed in the absorption of MB. This indicates that the presence of powder is necessary to induce an effect. The absorption signal measured on a suspension (powder + MB) kept in ambient conditions for 1 month shows no modification of the TiO signal while the signal due to MB has decreased, this suggests good stability of the powder. Figure 8 shows that after irradiation under UV light (340 nm, 3.65 eV), the A300C sample exhibits a stronger decrease of the methylene blue signal compared to the same test with TiO_2 P25. Still more interestingly, when the irradiation is shifted toward visible (430 nm, 2.89 eV), the A300C sample is still active toward methylene blue signal evolution while the TiO_2 P25 exhibits almost no activity. When irradiation is shifted to 530 nm (2.34 eV), once again the A300C sample is active toward methylene blue signal evolution. These observations can be correlated to the position of the optical gap of these two samples. This result is also interesting when compared to Dhumal[45]

(42) Gyorgy, E.; Perez del Pino, A.; Serra, P.; Morenza, J. L. *Surf. Coat. Technol.* **2003**, *173*, 265.
(43) Yang, J.; Bai, H.; Jiang, Q.; Lian, J. *Thin Solid Films* **2008**, *516*, 1736.
(44) Lee, S.; Jeon, C. *Chem. Mater.* **2004**, *16*, 4292.
(45) Dhumal, S.; Daulton, T.; Jiang, J.; Khonami, B.; Biswas, P. *Appl. Catal., B* **2009**, *86*, 145.

which shows that TiO_x ($x = 1.88-1.94$) oxygen deficient particles synthesized in a flame aerosol reactor exhibit activity in degradation of methyl orange solution under visible light illumination.

Conclusion

Finally, this paper has presented the synthesis at high temperature in the presence of a reducing atmosphere of an original Ti(O,N) free-standing nanopowder with a crystalline TiO contribution (average diameter 7 to 9 nm) in a rock-salt phase. The AF nanoparticles contain carbon removed by soft annealing treatment under air. A key point is the possibility of adjusting the optical gap down to 1.8 eV, which paves the way for applications where strong visible absorption is required. Interesting photoactivity has been demonstrated at 430 nm for the sample with the 1.8 eV gap. This low energy gap has been tentatively attributed to Ti(O, N) in a TiO rock-salt structure. More detailed studies of the evolution of local order will be carried out using EXAFS and low frequency infrared spectroscopy, and a more complete study of the photocatalytic activity including efficiency and stability tests on long duration experiments will be performed.

Acknowledgment. The authors thank the support of French program Namicercos from the MINEFI. We are also very grateful to our colleague Aurélie Habert for valuable help in characterizations. Jean Francois Tranchant and Véronique Guyot Ferréol from LVMH research are also gratefully acknowledged for fruitful discussions.